Supporting information for

"Structure-Function from the Outside In: Long-range Tertiary Contacts in RNA Exhibit Distinct Catalytic Roles"

Tara L. Benz-Moy and Daniel Herschlag

Table S1. Docking and coupling constants for WT and the P14 and MC/MCR mutants[a]

Construct	K_{dock}^{S} [b]	%S docked	$K_{dock}^{S_{-5U}}$ [c]	%S_{-5U} docked	$K_{dock}^{S'}$ [d]	$K_{dock}^{S'_{-5U}}$ [d]	Coupling S[e]	Coupling S_{-5U}[e]
WT	10.0	91	100	99	127	1200	13	12
P14 (L2)	2	67	20	95	7	85	4	4
P14 (L5c)	2	67	20	95	10	125	5	6
MC/MCR	0.5	33	5	83	0.9	13	2	3

[a] Mutants are labeled as in Figure 1. All values were determined as described in Materials and Methods. Reaction conditions: 30 °C, 10 mM $MgCl_2$, 50 mM Na•MOPS, pH 6.9.

[b] From Table 3.

[c] The docking value for S_{-5U} were obtained assuming that the 10-fold greater stabilization of docking for the WT ribozyme, relative to S (-1d,rSA_5), is maintained for the mutants (see *Measurement of UCG Affinities* in Materials and Methods).

[d] Determined from $(K_d^{UCG})_o$, $(K_d^{UCG})_c^{app}$, and K_{dock}^{S}(or $K_{dock}^{S\text{-}5U}$) according to eqn 5 in the main text (see *Measurement of UCG Affinities* in Materials and Methods).

[e] Determined from the ratio of $K_{dock}^{S'}/K_{dock}^{S}$ or $K_{dock}^{S\text{-}5U'}/K_{dock}^{S\text{-}5U}$ (eqn 4, see *Measurement of UCG Affinities* in Materials and Methods).

Table S2. Relative rate and equilibrium constants for the overall reaction and individual steps for the WT and mutant ribozymes[a]

A. Relative rate and equilibrium constants used to calculate $k_2^{overall}$ from eqns 11 and 13 in the main text

Construct	$K_{dock}^{S,rel}$ [b]	$(K_d^{UCG})_c^{rel}$ [c]	k_c^{rel} [b]	Calculated $k_2^{overall}$ [b]	Measured $k_2^{overall}$ [b]
WT	1	1	1	1	1
P13 (L2.1)	1.5	3.1	1.1	5.2	3.5
P13 (L9.1)	1.5	2.3	1.1	3.9	3.2
TL/TLR (L5b)	0.71	1.5	1.0	1.1	0.49
TL/TLR (J6a/b)	1.0	1.4	0.92	1.3	0.44
L9/P5	1.3	11.6	2.3	34.4	34.1

B. Relative rate and equilibrium constants used to calculate $k_2^{overall}$ from eqns 12 and 13 in the main text

Construct	$(K_d^{UCG})_o^{rel}$ [c]	$K_{dock}^{S',rel}$ [b]	k_c^{rel} [b]	Calculated $k_2^{overall}$ [b]	Measured $k_2^{overall}$ [b]
WT	1	1	1	1	1
P14 (L2)	0.71	16.7	1.8	21.3	18.0
P14 (L5c)	0.87	6.5	1.8	10.4	17.6
MC/MCR	1.4	62.4	1.7	148	63.7

[a] Mutants are labeled as in Figure 1. All values are relative to the WT from the measured values in Table 3 and were determined as described in the main text. Reaction conditions: 30 °C, 10 mM $MgCl_2$, 50 mM Na•MOPS, pH 6.9.

[b] Fold decrease from WT so that $k^{rel} = k^{WT}/k^{mutant}$, where k can be an equilibrium or rate constant.

[c] Fold increase from WT so that $k^{rel} = k^{mutant}/k^{WT}$, where k can be an equilibrium or rate constant.

[d] The value of $K_{dock}^{S',rel}$ for the P14(L2) and MC/MCR mutants assumes that these mutants have fully lost coupling between UCG and S as explained in Materials and Methods in the main text so that $K_{dock}^{S',rel} = 3 \times K_{dock}^{S,rel}$. The P14 (L5c) mutant is assumed to have lost half of the coupling between UCG and S so that $K_{dock}^{S',rel} = 1.5 \times K_{dock}^{S,rel}$ as explained in the Materials and Methods and the main text.

Table S3. Residues used to monitor folding of long-range tertiary contacts and the catalytic core via hydroxyl radical footprinting in Figure 4 in the main text (*1*)

Region monitored for folding	Residues
Catalytic core	57-60 94-97 108-111 272-275 279-282 298-301 310-313
P14	46-49 166-169
P13	68-81 347-350
MC/MCR	137-139 180-182 184-187 212
TL/TLR	151-153 250-253
L9/P5	118 327-329

Table S4. Dissociation constants for G and UCG for the WT and mutant ribozymes[a]

Construct	$(K_d^G)_c$ (μM)[b,c]	$(K_d^{UCG})_c$ (μM)[b,c]	$(K_d^G)_c/(K_d^{UCG})_c$ [c]
WT	88 ± 8[d]	3.0 ± 0.7[d]	29
P14 (L2)	≤271 ± 27	≤9 ± 1	44
P14 (L5c)	≤184 ± 37	≤8.1 ± 0.6	26
P13 (L2.1)	232 ± 16	10 ± 2	23
P13 (L9.1)	187 ± 9	7 ± 1	21
MC/MCR	≤507 ± 53	≤39 ± 2	21
TL/TLR (L5b)	135 ± 10	4 ± 1	34
TL/TLR (J6a/b)	160 ± 17	4.1 ± 0.6	39
L9/P5	≥600[e]	35 ± 17[d]	17

[a] Mutants are labeled as in Figure 1. The dissociation constant for G was determined using 0-2 mM G and a substrate that favors the closed complex for the WT ribozyme, -1d,rSA$_5$. The normalized binding curves for G are shown in Figure S4. The dissociation constants for UCG are from Table 3 (see also Figure S2A). Reactions were carried out as described in Materials and Methods. The ~30-fold weaker binding of G relative to UCG suggests that P9.0 is formed in all of the mutants. Reaction conditions: 30 °C, 10 mM $MgCl_2$, 50 mM Na•MOPS, pH 6.9.

[b] Errors are errors from the curve fit unless otherwise noted; the binding curve itself was generated once.

[c] The dissociation constants for the P14 and MC/MCR mutants are displayed as limits because these mutants significantly populate the open complex with substrates -1d,rSA$_5$ and -1d,rSA. The ratio between the dissociation constants for G and UCG assumes that the docking deficit is the same for -1d,rSA$_5$ and -1d,rSA so that the ratio between the dissociation constants provides a measure of P9.0 formation.

[d] Error is the standard deviation of two or more independent measurements.

[e] The dissociation constant for G binding to L9/P5 is a limit because clear saturation was not observed. The maximum rate at 2 mM G was used as k_{max} (eqn 3 in the main text) to obtain a limit for the value of $(K_d^G)_c$.

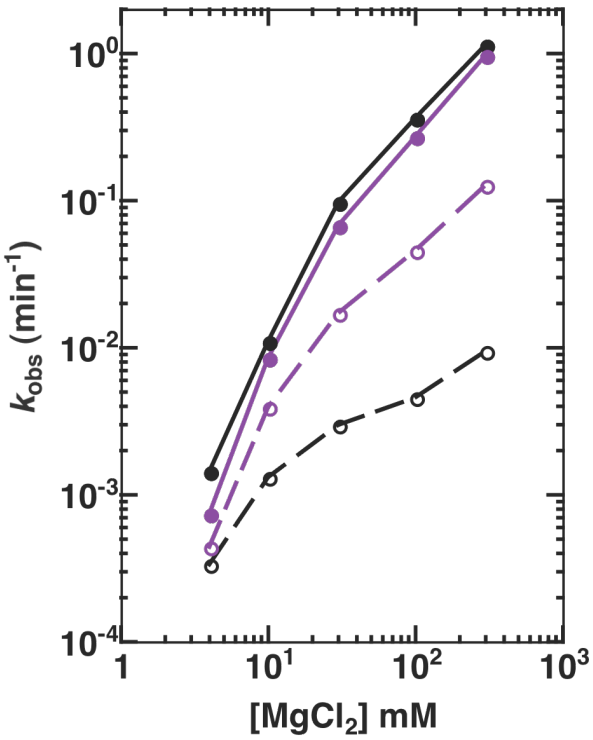

Figure S1. The observed rate constant of the guanosine-independent reaction for WT and the L9/P5 mutant as a function of [$MgCl_2$] compared to the corresponding observed rate constants of the guanosine-dependent reaction. The observed rate constant of the guanosine-independent reaction (open circles) is increased for the L9/P5 mutant (purple) relative to the WT (black). The observed rate constant of the guanosine-dependent reaction (k_{obs}) of $(E•S)_o$ + UCG → products (closed circles) was obtained at 10 μM UCG for WT (black) and 250 μM UCG for L9/P5 (purple) and are from Figure 3A. Reactions were carried out as described in the text and in Materials and Methods. Reaction conditions: 30 °C, 50 mM Na•MOPS, pH 6.9.

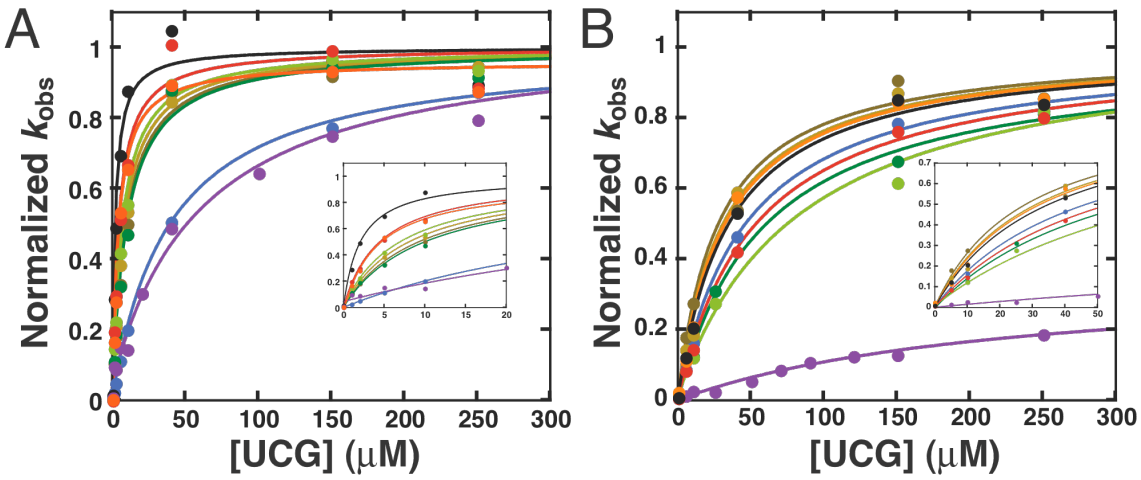

Figure S2. The UCG binding curves for both the open and closed complex substrates are superimposable for the majority of the mutant ribozymes. A. UCG binding curves with the closed complex substrate -1d,rSA. B. UCG binding curves with the open complex substrate, -1r,dSA$_5$. Inset shows the rates at lower concentrations of UCG overlay well for the majority of the mutants. For both parts A and B the majority of the curves overlay well and exhibit a plateau at the higher concentrations of UCG, suggesting that the UCG-dependent and inhibitory phases are well separated. The L9/P5 and MC/MCR mutants have curves that are notably different from the rest and suggest weaker binding of UCG, an effect that would not arise from additional inhibition at high concentrations of UCG. Reactions were carried out as described in Materials and Methods. The binding curves were normalized between 0 and 1 by subtracting the fitted guanosine-independent rate constant from each point and then dividing each point by the fitted maximal value, k_{max} (eqn 3). For the normalization of the L9/P5 mutant curve in part B which does not near saturation, the value of k_{max} was estimated to be 2-fold smaller than the WT value because $k_{max} = k_c K^S_{dock}$ for a substrate which favors the open complex, and for the L9/P5 mutant, k_c is affected ~2-fold and K^S_{dock} is unaffected (Table 3). Table 3 contains the measured UCG affinities for both A. and B. and the maximal fitted value for -1d,rSA in A. Colors are as in Figure 1: WT (**black**); P13 mutants (L2.1: **dark green**, L9.1: **olive green**); P14 mutants (L2: **brown**; L5c: **tan**); MC/MCR mutant (**blue**); TL/TLR mutants (L5b: **red-orange**; J6a/b: **light orange**); L9/P5 mutant (**purple**). Reaction conditions: 30 °C, 10 mM $MgCl_2$, 50 mM Na•MOPS, pH 6.9.

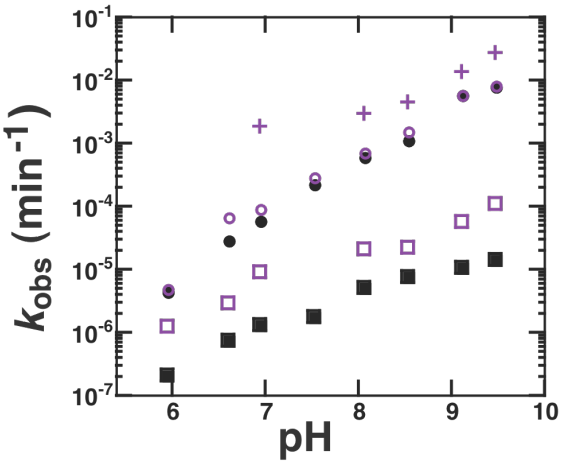

Figure S3. The pH dependence of the reaction of E•-1d,rSA$_5$ + G → P (circles) and E•-1d,rSA$_5$ → P (squares) for the WT ribozyme (black) and the L9/P5 mutant (purple). All of the WT ribozyme and >90% of the L9/P5 mutant react slower in the guanosine-independent reaction (squares) than in the measured guanosine-dependent reaction (circles). The guanosine-dependent reaction is from Figure 7B. As noted in the main text, the L9/P5 guanosine-independent reaction exhibited biphasic kinetics (at pH ≥7, in this case), and <10% of the L9/P5 mutant exhibited a guanosine-independent burst reaction that was faster than the measured guanosine-dependent reaction (purple crosses). Concentrations of G at or above 50 μM eliminate measurable biphasic kinetics for the L9/P5 mutant, suggesting that this fast phase is not significantly contributing to the guanosine-dependent reaction under the observation conditions. The concentration of G in the reaction was subsaturating: 10 μM G (WT) and 300 μM G (L9/P5). The ribozyme concentration was 50 nM and saturating with respect to S. Reaction conditions: 5 °C, 10 mM $MgCl_2$, 50 mM buffer (see Materials and Methods for buffer identities).

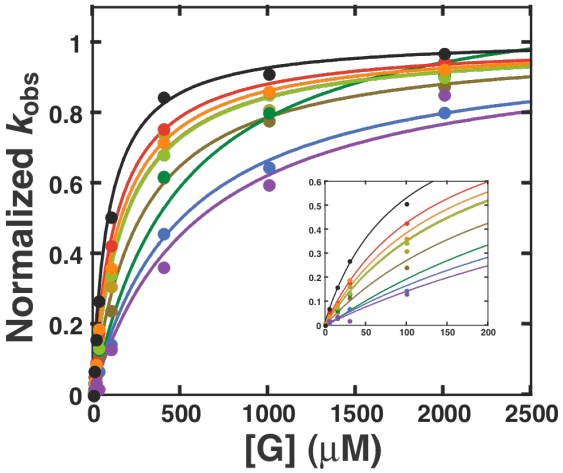

Figure S4. The G binding curves for the closed complex substrate -1d,rSA$_5$. Inset shows the observed rates at lower concentrations of G. G affinities are from Table S4. Reactions contained 0-2 mM G and the substrate -1d,rSA$_5$ that favors the closed complex with WT ribozyme and were carried out as described in Materials and Methods. The binding curves were normalized between 0 and 1 by subtracting the fitted guanosine-independent rate consant from each point and then dividing each point by the fitted maximal value, k_{max} (eqn 3). For the normalization of L9/P5 mutant curve, k_{max} was estimated to be 2-fold smaller than the WT value because this value should represent k_c for a substrate that favors the closed complex, and for the L9/P5 mutant k_c is affected 2-fold (Table 3). Colors are as in Figure 1: WT (**black**); P13 mutants (L2.1: **dark green**, L9.1: **olive green**); P14 mutants (L2: **brown**; L5c: **tan**); MC/MCR mutant (**blue**); TL/TLR mutants (L5b: **red-orange**; J6a/b: **light orange**); L9/P5 mutant (**purple**). Reaction conditions: 30 °C, 10 mM $MgCl_2$, 50 mM sodium•MOPS, pH 6.9.

Analysis of Hydroxyl Radical Footprinting Data for the Folded WT versus Mutant Ribozymes

The following text and figures provide an example of the analysis of footprinting data described in *Hydroxyl radical footprinting with Fe(II)-EDTA* in the Materials and Methods. The footprinting data collected for the MC/MCR mutant alongside the WT ribozyme are shown throughout as an example for each step of the analysis. While there are of necessity ad hoc aspects to the analysis as all of the sources of error are not understood, this systematic approach and defined cut-offs are preferable to the common approach of determining positions of difference by visual gel inspection or by analysis of comparisons on single gels.

1. *Raw Data (Figure S5).* The SAFA output (*2*), the area under the curve for each residue from a plot of arbitrary counts versus residue, was plotted for each footprinting reaction for each gel (Figure S5). The data for three to five footprinting reactions for a single RNA on a single gel were overlaid. The raw data overlay reasonably well but exhibit some differences in the intensity of the cleavage pattern for a given reaction (e.g., see Figure S5A, purple trace & Figure S5B, red trace). The purple trace in Figure S5A shows aberrant signal at multiple positions and was therefore removed from the rest of the data analysis. In the entire dataset for the MC/MCR mutant, only 2 of 82 total gel lanes were discarded. The red trace in Fig. S5B appears to have had less radiolabeled RNA loaded onto the gel than the other traces for the MC/MCR mutant. The normalization procedures in steps 2 and 3 reduce these differences among the traces so that the red trace in Figure S5B can be overlaid with the other traces. The different gels vary in the number of residues that can be resolved, and, therefore, limits of resolution must be determined for each gel (see step 3 below). Only data within these limits of resolution were used in the analysis subsequent to the initial *Max/Min Normalization & Solver* in step 3. These cutoffs are displayed as red dashed lines in Figure S5 and are further discussed in step 3.

2. *Max/Min Normalization (Figure S6).* To reduce the differences among the footprinting traces for the raw data, each trace was normalized between -1 and 1 (eqn 8 in the main text) for residues within the limits of resolution for the data (Figure S6). While the limits of resolution are more strictly defined in step 3, the limits of resolution were defined more conservatively in step 2 as the set of bands that could be resolved by eye in the gel. The three residue positions that give the highest cleavage (defined as curve areas in SAFA) were averaged (these are typically within ~20% of each other) to give a maximum value of cleavage for a residue that is solvent exposed (abbreviated 'max' in eqn 8), and the three correspondingly lowest cleavage residues (typically within ~40% of each other) were averaged together to give a minimum value of cleavage for a residue that is minimally solvent exposed (abbreviated 'min' in eqn 8). Note that any limitations in the normalization procedure will lead to greater standard deviations for the extent of cleavage at individual positions and therefore lower significance, in

keeping with our conservative approach to identifying positions of differential cleavage that is used throughout.

3. *Max/Min Normalization & Solver (Figure S7)*. To further reduce systematic differences between the individual curves from the footprinting reactions for a single RNA, the program Solver (Frontline Systems), which runs within Microsoft Excel, was used to minimize the differences between the curves by minimizing the sum of the variances of the average of the single footprinting curves for a single RNA (Figure S7). The variances are minimized by allowing the max/min values from step 2 to be varied within a reasonable range (typically, within 30% of the initial max/min value determined by averaging). After completion of this step, the limits of resolution used for the subsequent steps were determined. The limits of resolution were determined visually by the positions at which the normalized curve areas no longer overlay well. Once regions overlay less well, they can become much more noisy, as in data 3′ to the dashed red line in Figure S7C & D, or they can become only slightly more noisy and maintain the general features of the footprint (Figure S7A and B). Even if the general features are maintained, the resolution of the data by nucleotide becomes worse outside of the limits of resolution (compare data for nucleotides ~180-185 in Figure S8A below with those Figure 8D in the main text). The limits of resolution are defined by the data that are 5′ to the dashed red line in Figure S7 for 5′-labeled RNA and are similarly defined towards the 3′-end for a 3′-labeled RNA. After this step, other visually aberrant footprinting residue positions or entire footprinting reactions are removed from the analysis; these positions presumably arise due to occasional spurious events from sporadic nuclease exposure or other unrecognized events (*3, 4*). In this example analysis, Figure S7B contains a few residues that were removed from the analysis for certain traces for MC/MCR; the removed residues are denoted by colored numbers.

4. *Averaging of single footprinting traces (Figure S8)*. To allow comparison between the mutants and the WT, the single footprinting traces for a single RNA from step 3 are combined to give an averaged footprinting trace. The standard deviations for each residue within this trace were determined by the standard equations. Solver was used to minimize the square of the difference between the traces for the WT and MC/MCR ribozymes concurrently with the minimization in step 3. An overlay of the MC/MCR average trace and the WT trace are shown in Figure S8. At this step, differences between averaged traces for the MC/MCR mutant and the WT within a single gel can be deciphered. However, day-to-day variation in the absolute cleavage differences between WT and the mutants do not allow simple comparison across gels. The next steps in the analysis allow comparison across gels.

5. *Determining the difference between the WT and mutant averaged traces (Figure S9)*. The averaged mutant trace was subtracted from the averaged WT trace,

producing a difference trace (Figure S9). Within this difference trace, nucleotides for the mutant that are more cleaved than WT are negative values, and nucleotides for the mutant that are less cleaved than WT are positive values. The errors shown for each of the difference traces are the errors propagated as is appropriate for the subtraction of two values each with their own standard deviations.

6. *Averaging the difference traces for each mutant (Figure S10).* To determine the differences in hydroxyl radical cleavage between the WT and mutant, the difference traces within the limits of resolution for all of the gels for a mutant were averaged (Figure S10 for the MC/MCR mutant and Figures S11-S17 for the other mutants). Typically, eight gels were averaged (two independent sets of 2- and 4-hour gels with 5′-labeled RNA and two independent sets 2- and 4-hour gels with 3′-labeled RNA). As stated above, the absolute differences between the WT and mutant ribozymes varied from day-to-day, but the difference itself should remain after averaging the differences, and the generally small error bars for these averaged values supports this point. The errors on the single difference traces were propagated as is appropriate for averaged values, and these propagated errors are displayed with average difference values in Figure S10.

7. *Determining positions of different hydroxyl radical cleavage between the mutant and WT (Figures S10-S17).* The averaged differences in hydroxyl radical cleavage between the mutant and WT exhibit some modest baseline variation around '0' (Figures S10-S17). To determine the signal from the noise, a cutoff was applied to these averaged differences. This cutoff was chosen conservatively to recapitulate of most of the differences that were consistently observed between WT and mutant in a single gel. Averaged differences greater than 0.2 or less than -0.2 were considered significant if the following held: a) They clustered in a group of two or more nucleotides, separated by no more than one value that is not significantly beyond the cutoff. b) The error bars of the averaged difference at a residue did not contact or cross the 0.2 or -0.2 value; otherwise that nucleotide was considered to be not significantly different from the WT. c) A residue not in a cluster was only considered to be significantly different than WT if its value was greater than 0.6 or less than -0.6 and had error bars that did not contact or cross the 0.6 or -0.6 value. This difference in cutoff for a single nucleotide versus a cluster of nucleotides was chosen because it was observed that systematic errors in a gel or gel set could occasionally show up in the differences as false positives by the 0.2 cutoff for non-clustered nucleotides.

Figure Captions for the Analysis of Hydroxyl Radical Footprinting Data for the Folded WT versus Mutant Ribozymes

Figure S5. The raw SAFA output for the 5′-labeled MC/MCR and WT ribozymes from the 2-hour gels (step 1; see *Hydroxyl radical footprinting with Fe(II)-EDTA* in Materials and Methods). The different colors represent different footprinting reactions, and the term "Gel Set" refers to a set of gels that were run for 2- and 4-hours with the same footprinting reactions loaded onto them. Each residue 5′ to the red dashed line is used in the final analysis; the dashed red line denotes the limit of resolution for each data set. Conditions: 25 °C, 10 mM $MgCl_2$, 50 mM sodium•MOPS, pH 6.9.

Figure S6. Initial normalization of the 5′-labeled MC/MCR and WT ribozymes from the 2-hour gels (step 2). All colors, terms, representations, and conditions are as described in Figure S5.

Figure S7. Additional normalization of the 5′-labeled MC/MCR and WT ribozymes (step 3) from the gels that were run for 2-hours using the computer program Solver. The colored numbers in B denote nucleotides that were removed from the final analysis of the data for the dataset of the corresponding color. All other colors, terms, representations, and conditions are as described in Figure S5.

Figure S8. The average values of hydroxyl radical cleavage for the 5′-labeled MC/MCR and WT ribozymes (step 4) from the gels that were run for 2-hours. The ribozymes are colored as in Figure 1 (WT: black; the MC/MCR mutant: blue). The error bars represent standard deviations from the different footprinting reactions (the colored reactions in Figures S5-S7). All other terms, representations, and conditions are as described in Figure S5.

Figure S9. The difference between the averaged values of the 5′-labeled MC/MCR and WT ribozymes (step 5) from the gels that were run for 2-hours. The values for the MC/MCR mutant were subtracted from those of WT. The error bars represent the

propagated error from subtraction of the averaged values for the MC/MCR and WT ribozymes. All other terms, representations, and conditions are as described in Figure S5.

Figure S10. The average differences in hydroxyl radical cleavage between the MC/MCR and WT ribozymes (steps 6 & 7). The gray dashed lines are positioned at the cutoff values of 0.2 and -0.2, and the black dashed lines are positioned at the cutoff values of 0.6 and -0.6. The error bars represent the propagated errors from average of the (WT-Mutant) differences across gels. Thick red bars indicate areas determined to be areas of altered cleavage in the MC/MCR mutant compared to the WT as displayed in Figure 8D of the main text. Data from nine gels was used to obtain this plot. Conditions: 25 °C, 10 mM $MgCl_2$, 50 mM Na•MOPS, pH 6.9.

Figure S11. The differences in hydroxyl radical cleavage between the P13 (L2.1) and WT ribozymes. Thick red bars indicate areas determined to be areas of altered cleavage in the P13 (L2.1) mutant compared to the WT as displayed in Figure 8A of the main text. Thick black bars indicate areas of cleavage in the mutation site that cannot be directly compared to the WT because the mutation alters the length of the construct. Data from eight gels was used to obtain this plot. Methods for difference determination, representations, and conditions are as described in Figure S10.

Figure S12. The differences in hydroxyl radical cleavage between the P13 (L9.1) and WT ribozymes. Thick red bars indicate areas determined to be areas of altered cleavage in the P13 (L9.1) mutant compared to the WT as displayed in Figure 8A of the main text. Data from eight gels was used to obtain this plot. Methods for difference determination, representations, and conditions are as described in Figure S10.

Figure S13. The differences in hydroxyl radical cleavage between the TL/TLR (L5b) and WT ribozymes. Thick red bars indicate areas determined to be areas of altered cleavage in the TL/TLR (L5b) mutant compared to the WT as displayed in Figure 8B of the main text. Data from six gels was used to obtain this plot. Methods for difference determination, representations, and conditions are as described in Figure S10.

Figure S14. The differences in hydroxyl radical cleavage between the TL/TLR (J6a/b) and WT ribozymes. Thick red bars indicate areas determined to be areas of altered cleavage in the TL/TLR (J6a/b) mutant compared to the WT as displayed in Figure 8B of the main text. Thick gray bars indicate nucleotides that exhibited low background cleavage in the untreated lane for the J6a/b mutant and were thrown out of the analysis because of the small number of gels obtained for this mutant. Data from four gels was used to obtain this plot. Methods for difference determination, representations, and conditions are as described in Figure S10.

Figure S15. The differences in hydroxyl radical cleavage between the P14 (L2) and WT ribozymes. Thick red bars indicate areas determined to be areas of altered cleavage in the P14 (L2) mutant compared to the WT as displayed in Figure 8C of the main text. Data from eight gels was used to obtain this plot. Methods for difference determination, representations, and conditions are as described in Figure S10.

Figure S16. The differences in hydroxyl radical cleavage between the P14 (L5c) and WT ribozymes. Thick red bars indicate areas determined to be areas of altered cleavage in the P14 (L5c) mutant compared to the WT as displayed in Figure 8C of the main text. Data from eight gels was used to obtain this plot. Methods for difference determination, representations, and conditions are as described in Figure S10.

Figure S17. The differences in hydroxyl radical cleavage between the L9/P5 and WT ribozymes. Thick red bars indicate areas determined to be areas of altered cleavage in the L9/P5 mutant compared to the WT as displayed in Figure 8C of the main text. Data from eleven gels was used to obtain this plot. Methods for difference determination, representations, and conditions are as described in Figure S10.

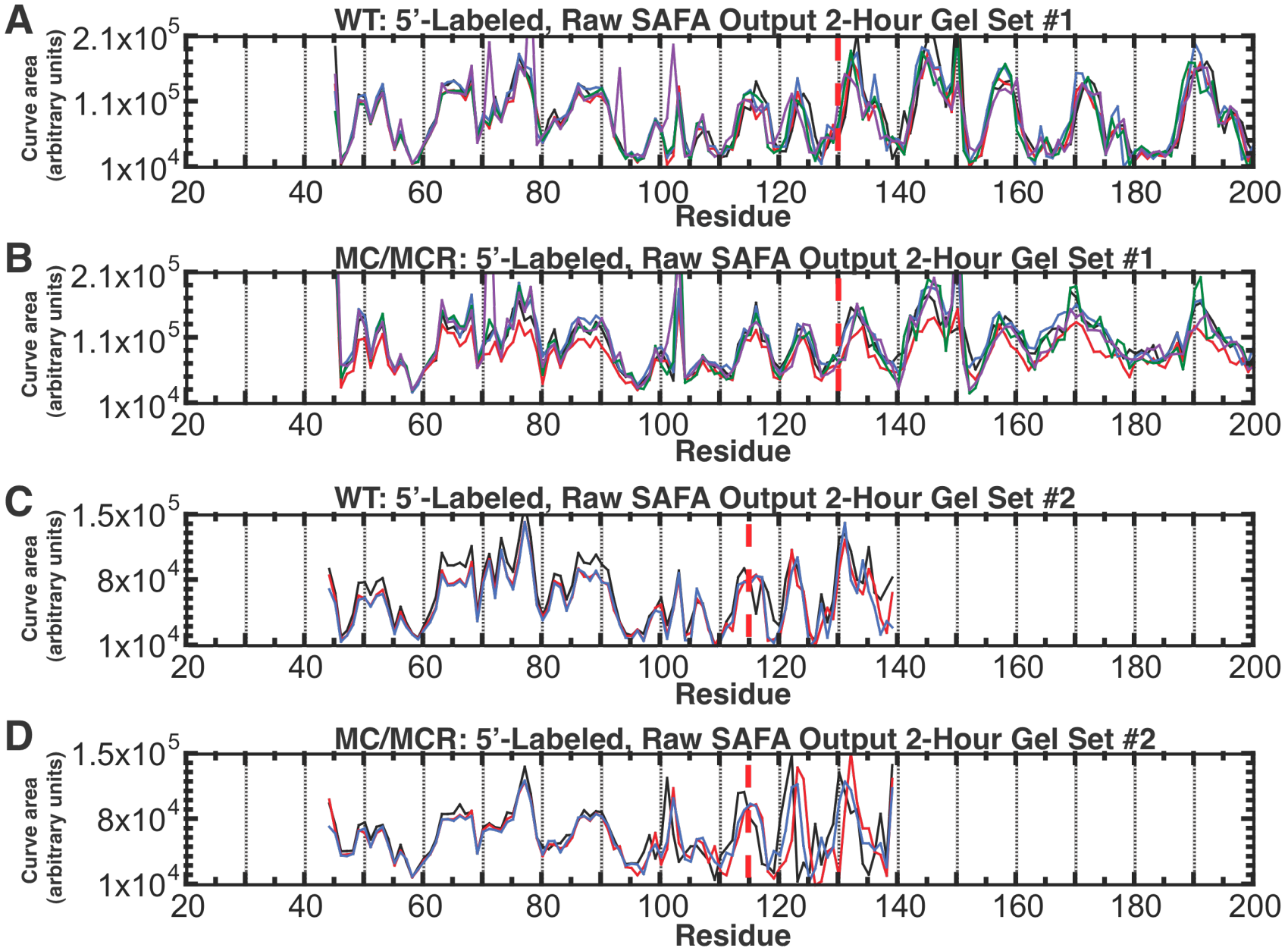
A
WT: 5'-Labeled, Raw SAFA Output 2-Hour Gel Set #1
Curve area (arbitrary units)
2.1x10^5
1.1x10^5
1x10^4
20 40 60 80 100 120 140 160 180 200
Residue
B
MC/MCR: 5'-Labeled, Raw SAFA Output 2-Hour Gel Set #1
Curve area (arbitrary units)
2.1x10^5
1.1x10^5
1x10^4
20 40 60 80 100 120 140 160 180 200
Residue
C
WT: 5'-Labeled, Raw SAFA Output 2-Hour Gel Set #2
Curve area (arbitrary units)
1.5x10^5
8x10^4
1x10^4
20 40 60 80 100 120 140 160 180 200
Residue
D
MC/MCR: 5'-Labeled, Raw SAFA Output 2-Hour Gel Set #2
Curve area (arbitrary units)
1.5x10^5
8x10^4
1x10^4
20 40 60 80 100 120 140 160 180 200
Residue

Figure S5

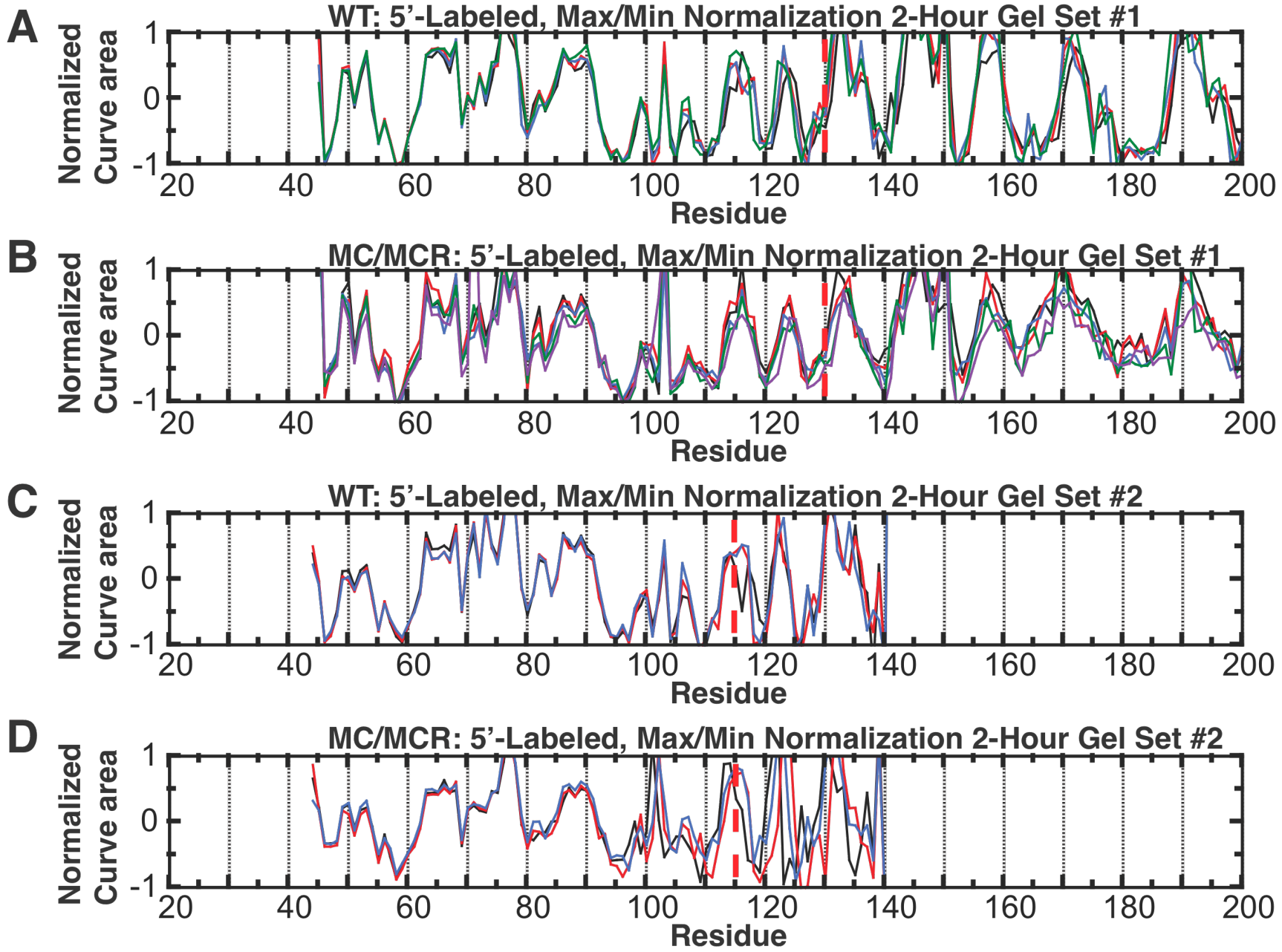
A
WT: 5'-Labeled, Max/Min Normalization 2-Hour Gel Set #1
Normalized Curve area
1
0
-1
20
40
60
80
100
120
140
160
180
200
Residue
B
MC/MCR: 5'-Labeled, Max/Min Normalization 2-Hour Gel Set #1
Normalized Curve area
1
0
-1
20
40
60
80
100
120
140
160
180
200
Residue
C
WT: 5'-Labeled, Max/Min Normalization 2-Hour Gel Set #2
Normalized Curve area
1
0
-1
20
40
60
80
100
120
140
160
180
200
Residue
D
MC/MCR: 5'-Labeled, Max/Min Normalization 2-Hour Gel Set #2
Normalized Curve area
1
0
-1
20
40
60
80
100
120
140
160
180
200
Residue

Figure S6

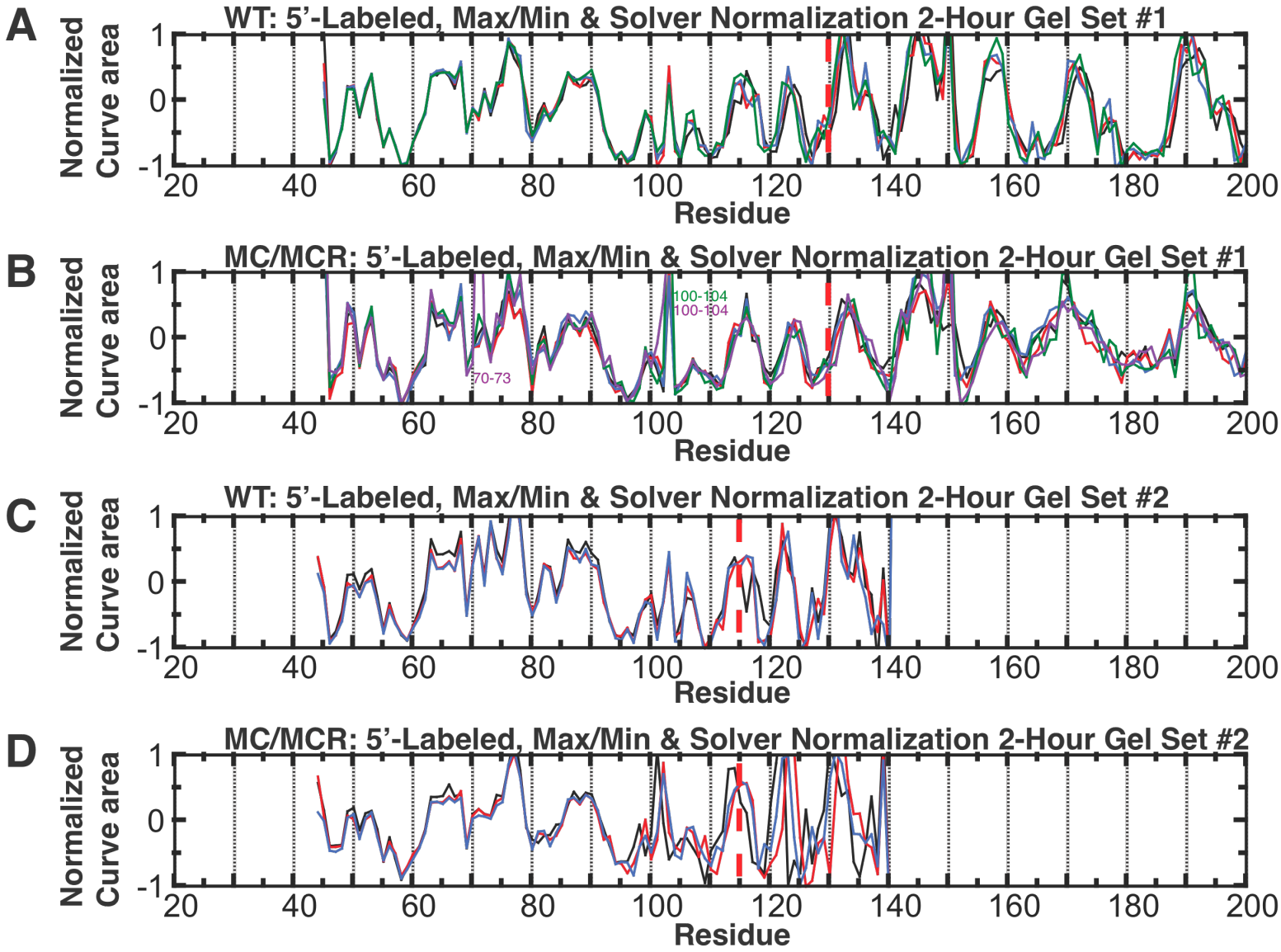
A
WT: 5'-Labeled, Max/Min & Solver Normalization 2-Hour Gel Set #1
B
MC/MCR: 5'-Labeled, Max/Min & Solver Normalization 2-Hour Gel Set #1
100-104
100-104
70-73
C
WT: 5'-Labeled, Max/Min & Solver Normalization 2-Hour Gel Set #2
D
MC/MCR: 5'-Labeled, Max/Min & Solver Normalization 2-Hour Gel Set #2
Normalized Curve area
Residue
1
0
-1
20
40
60
80
100
120
140
160
180
200

Figure S7

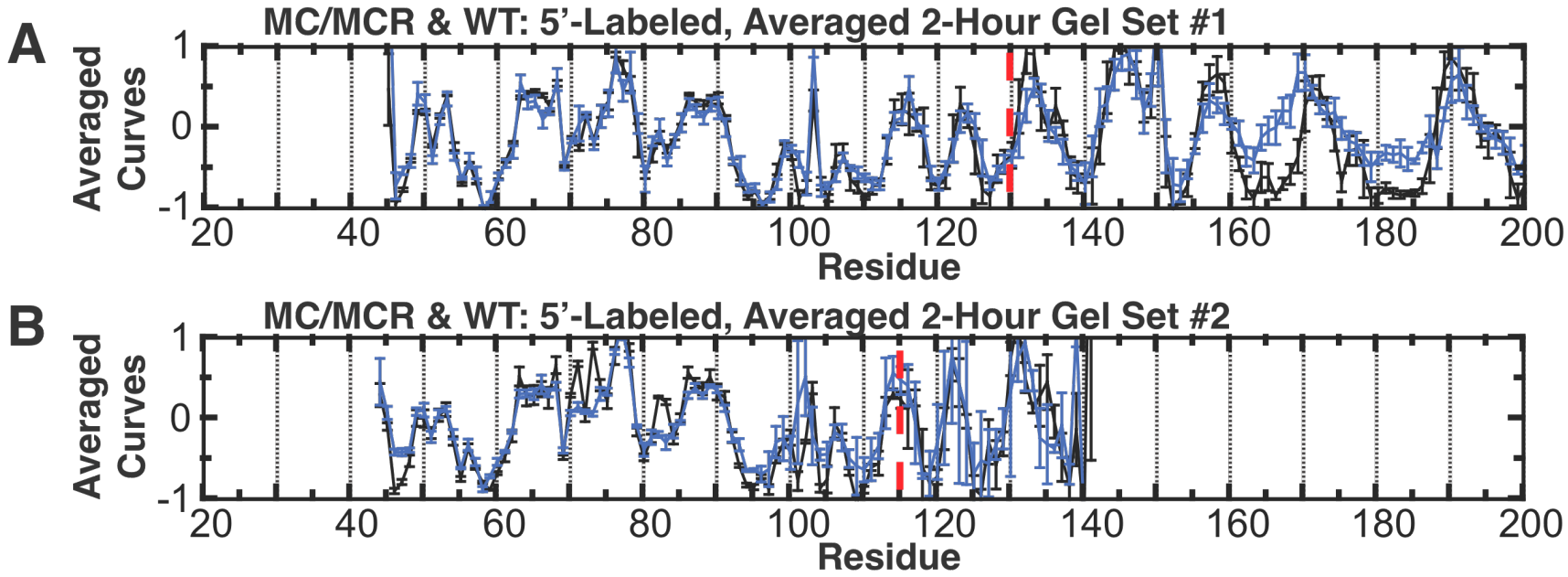
A
MC/MCR & WT: 5'-Labeled, Averaged 2-Hour Gel Set #1
Averaged Curves
1
0
-1
20
40
60
80
100
120
140
160
180
200
Residue
B
MC/MCR & WT: 5'-Labeled, Averaged 2-Hour Gel Set #2
Averaged Curves
1
0
-1
20
40
60
80
100
120
140
160
180
200
Residue

Figure S8

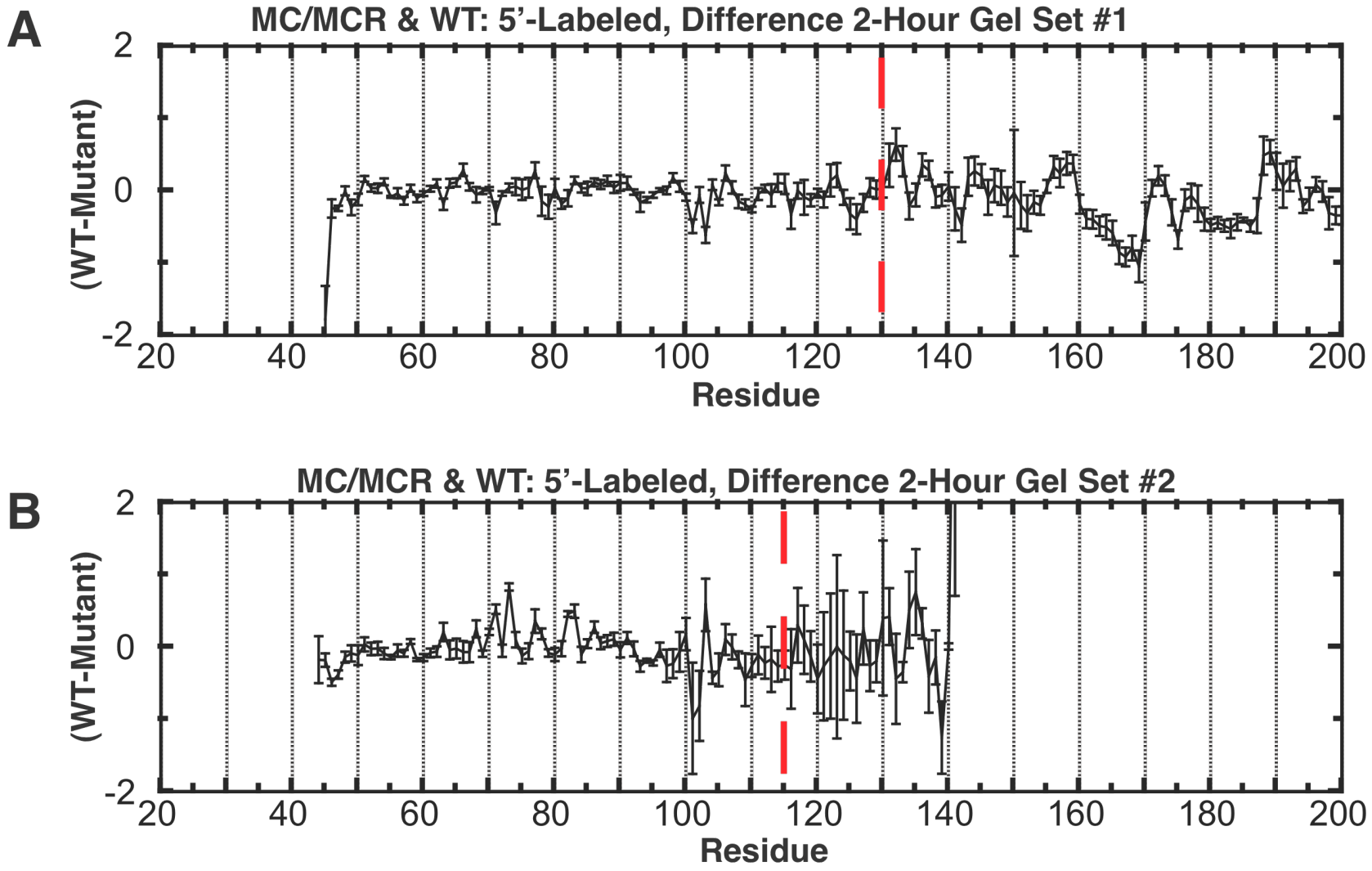
A
MC/MCR & WT: 5'-Labeled, Difference 2-Hour Gel Set #1
(WT-Mutant)
2
0
-2
20
40
60
80
100
120
140
160
180
200
Residue
B
MC/MCR & WT: 5'-Labeled, Difference 2-Hour Gel Set #2
(WT-Mutant)
2
0
-2
20
40
60
80
100
120
140
160
180
200
Residue

Figure S9

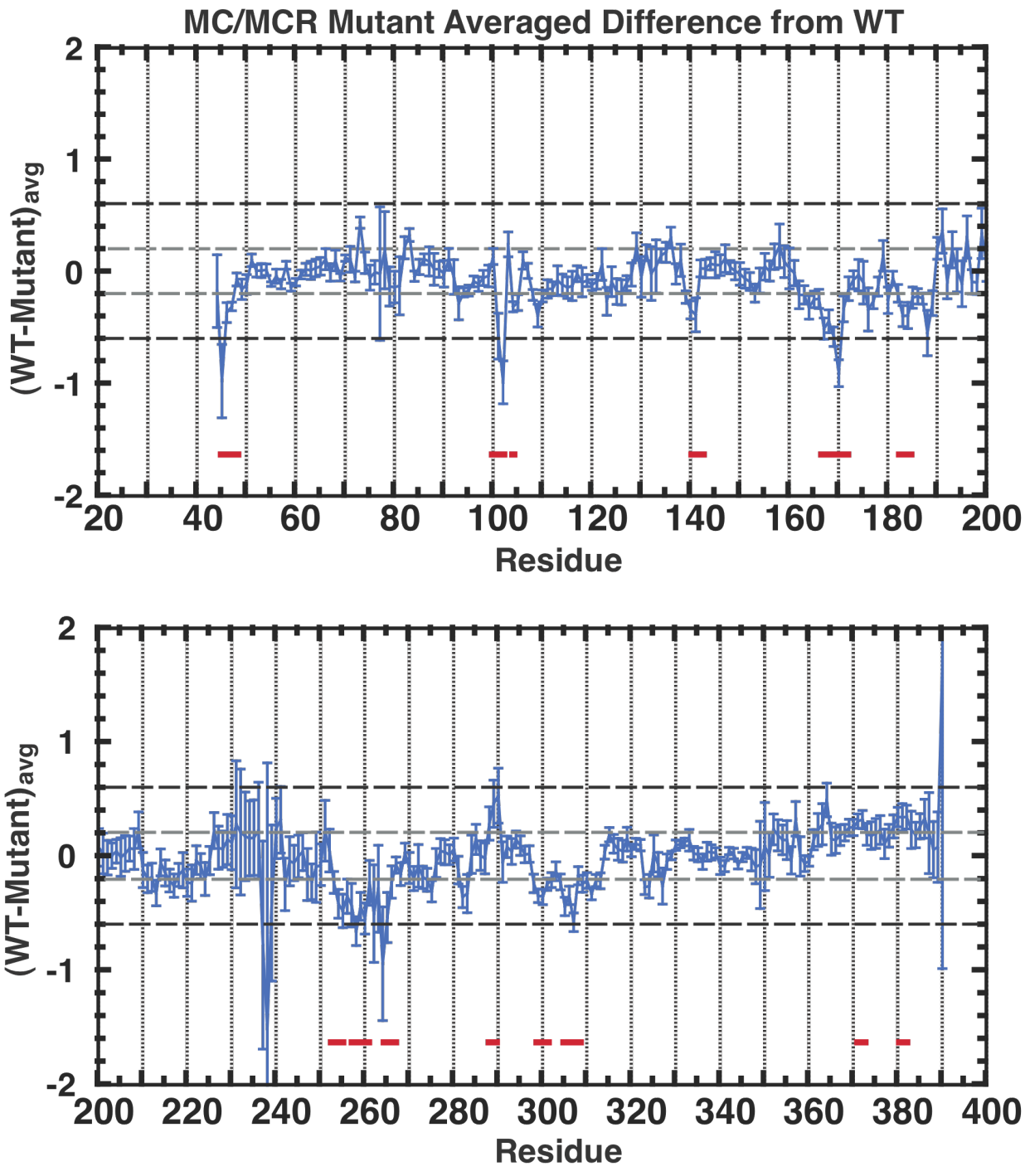
MC/MCR Mutant Averaged Difference from WT
(WT-Mutant)avg
Residue
2
1
0
-1
-2
20
40
60
80
100
120
140
160
180
200
220
240
260
280
300
320
340
360
380
400

Figure S10

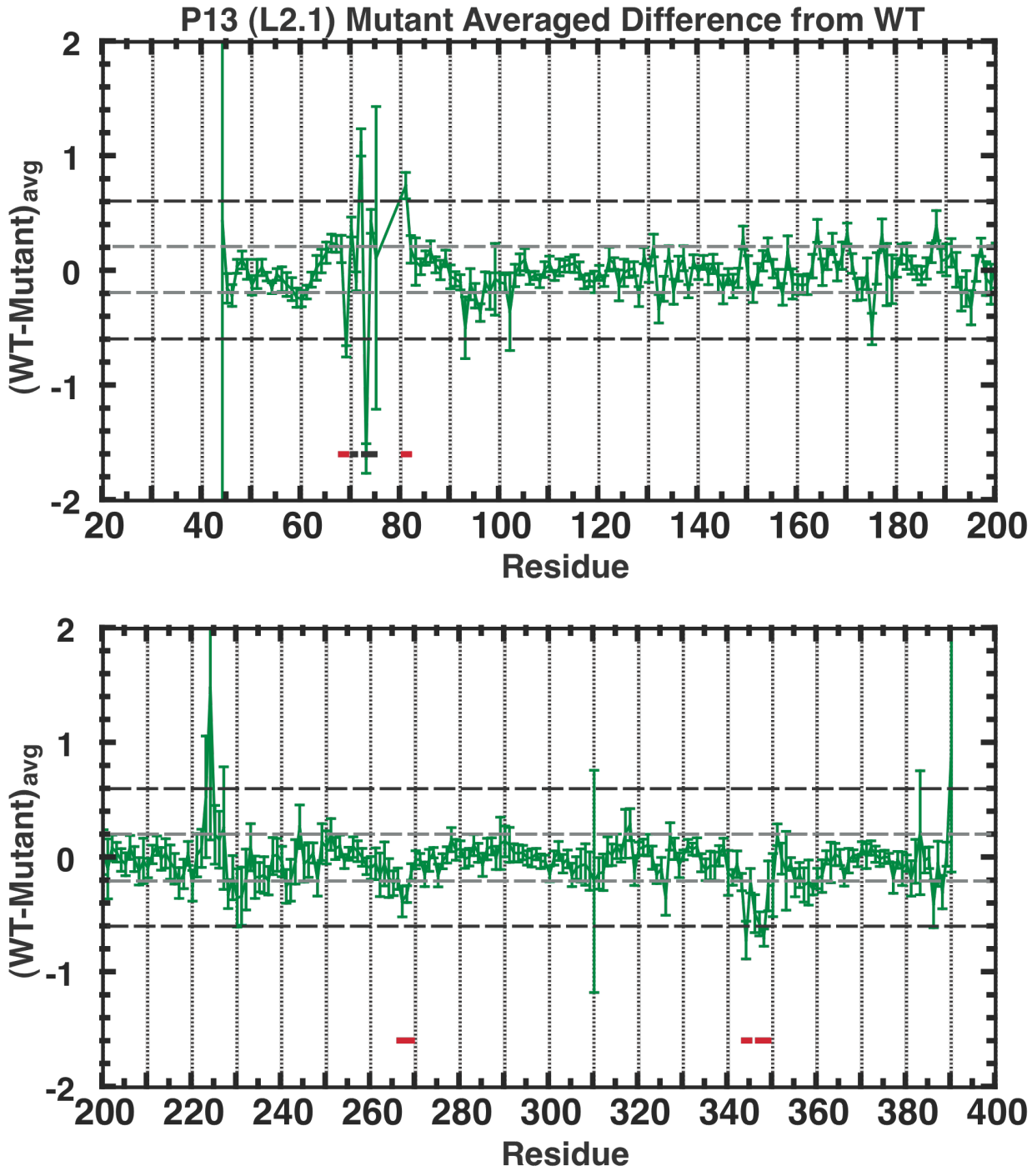
P13 (L2.1) Mutant Averaged Difference from WT
(WT-Mutant)avg
Residue
2
1
0
-1
-2
20
40
60
80
100
120
140
160
180
200
220
240
260
280
300
320
340
360
380
400

Figure S11

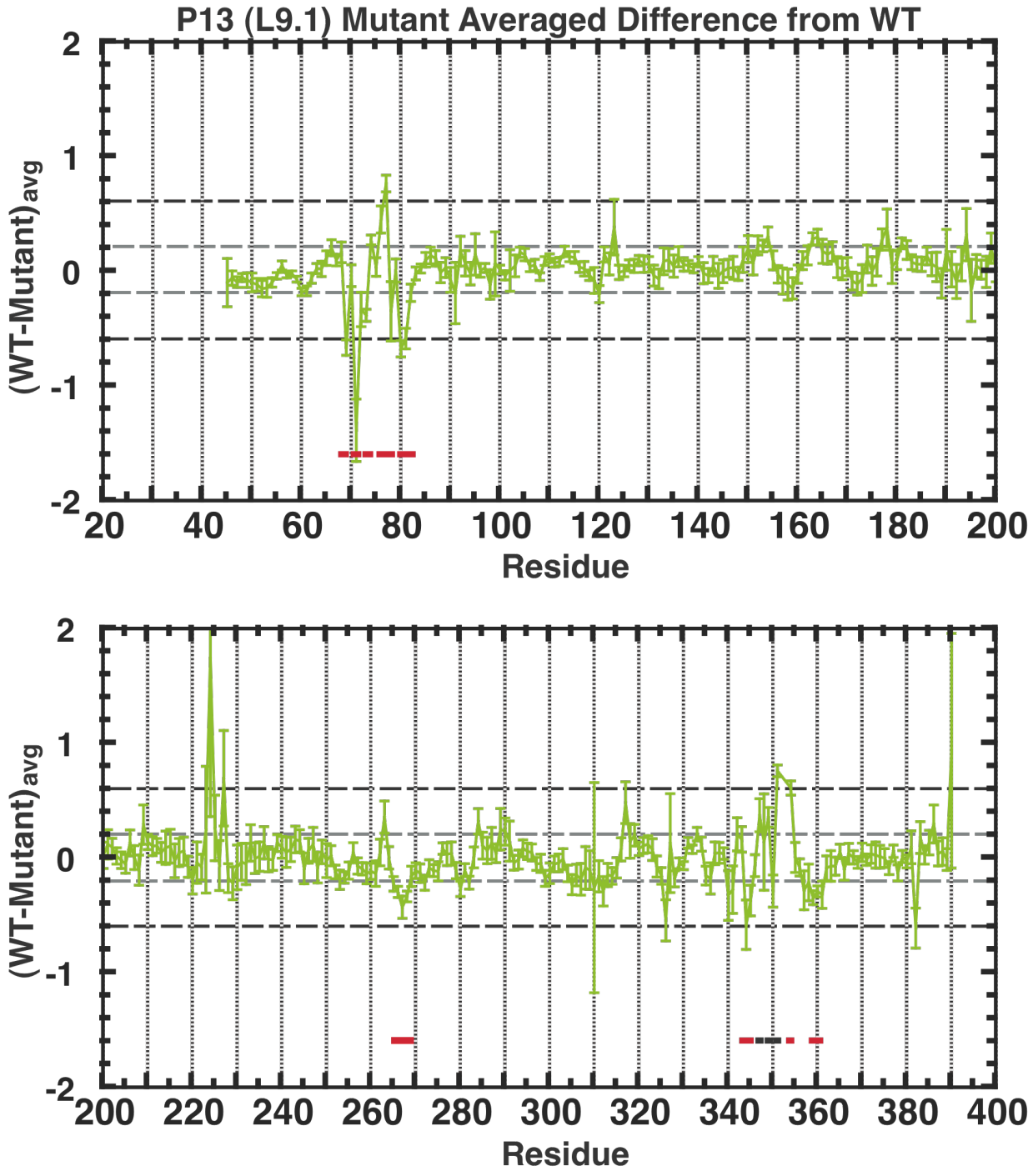
P13 (L9.1) Mutant Averaged Difference from WT
(WT-Mutant)avg
Residue
2
1
0
-1
-2
20
40
60
80
100
120
140
160
180
200
(WT-Mutant)avg
Residue
2
1
0
-1
-2
200
220
240
260
280
300
320
340
360
380
400

Figure S12

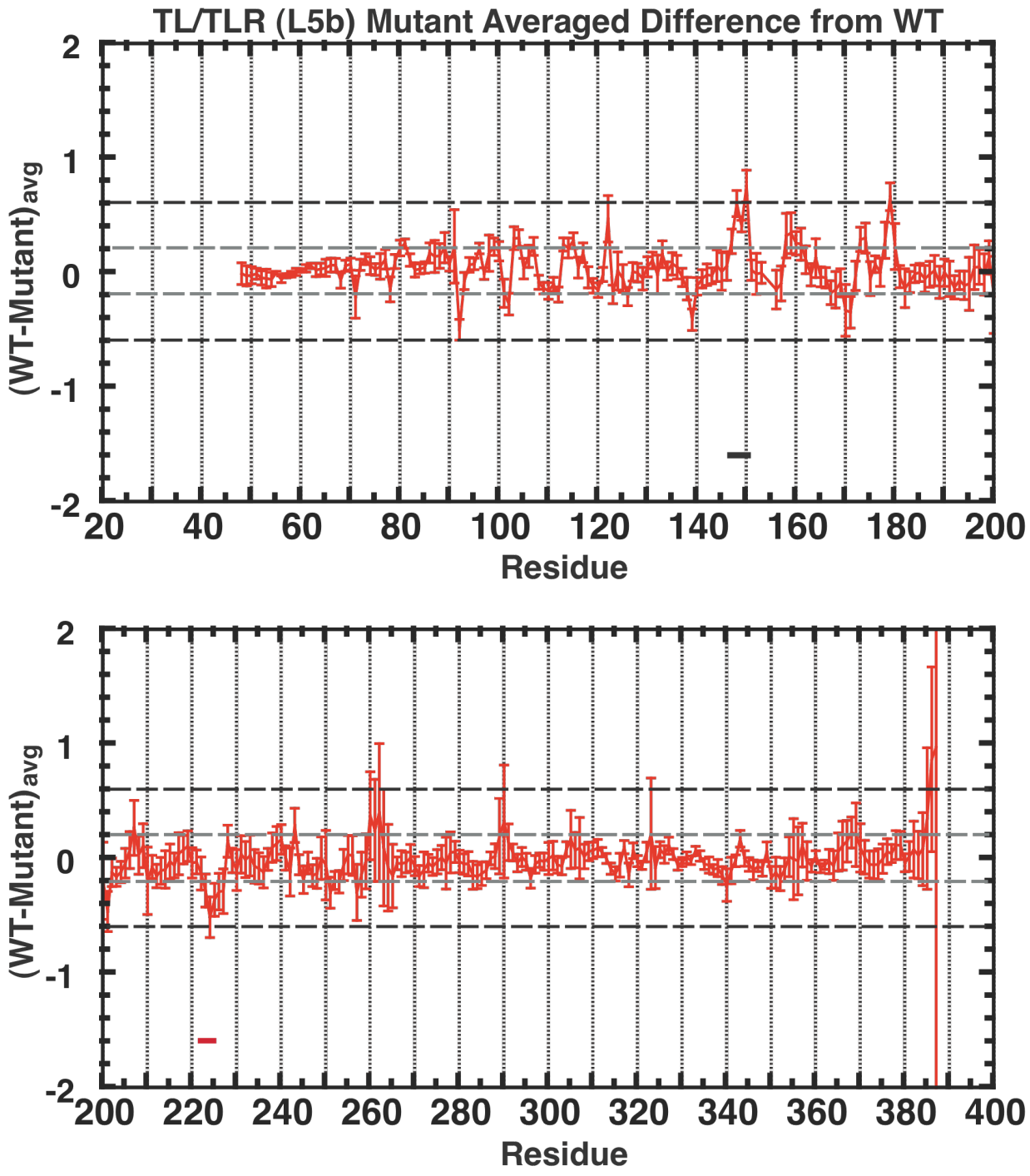
TL/TLR (L5b) Mutant Averaged Difference from WT
(WT-Mutant)avg
Residue
2
1
0
-1
-2
20
40
60
80
100
120
140
160
180
200
220
240
260
280
300
320
340
360
380
400

Figure S13

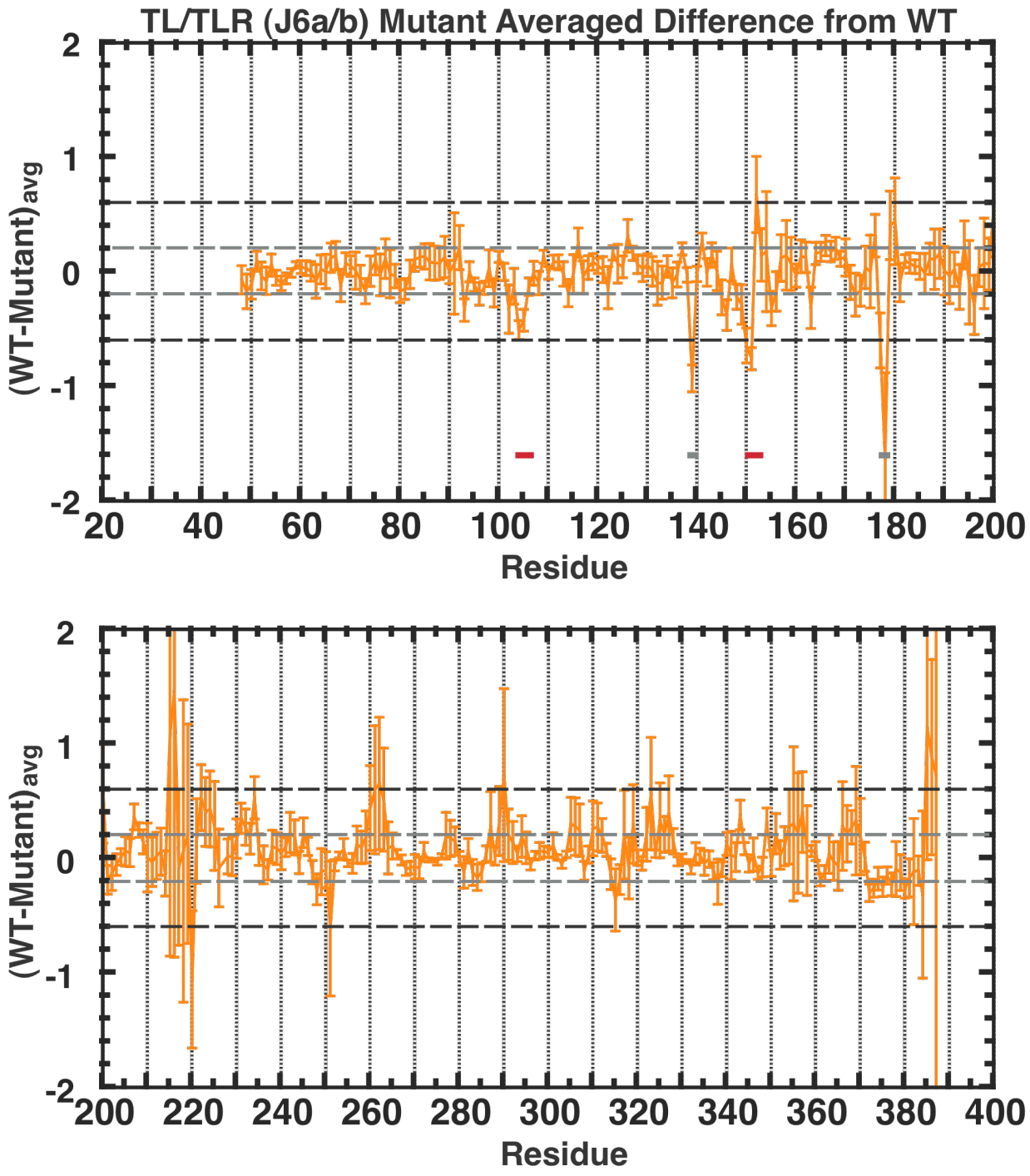
TL/TLR (J6a/b) Mutant Averaged Difference from WT
(WT-Mutant)avg
Residue
2
1
0
-1
-2
20
40
60
80
100
120
140
160
180
200
220
240
260
280
300
320
340
360
380
400

Figure S14

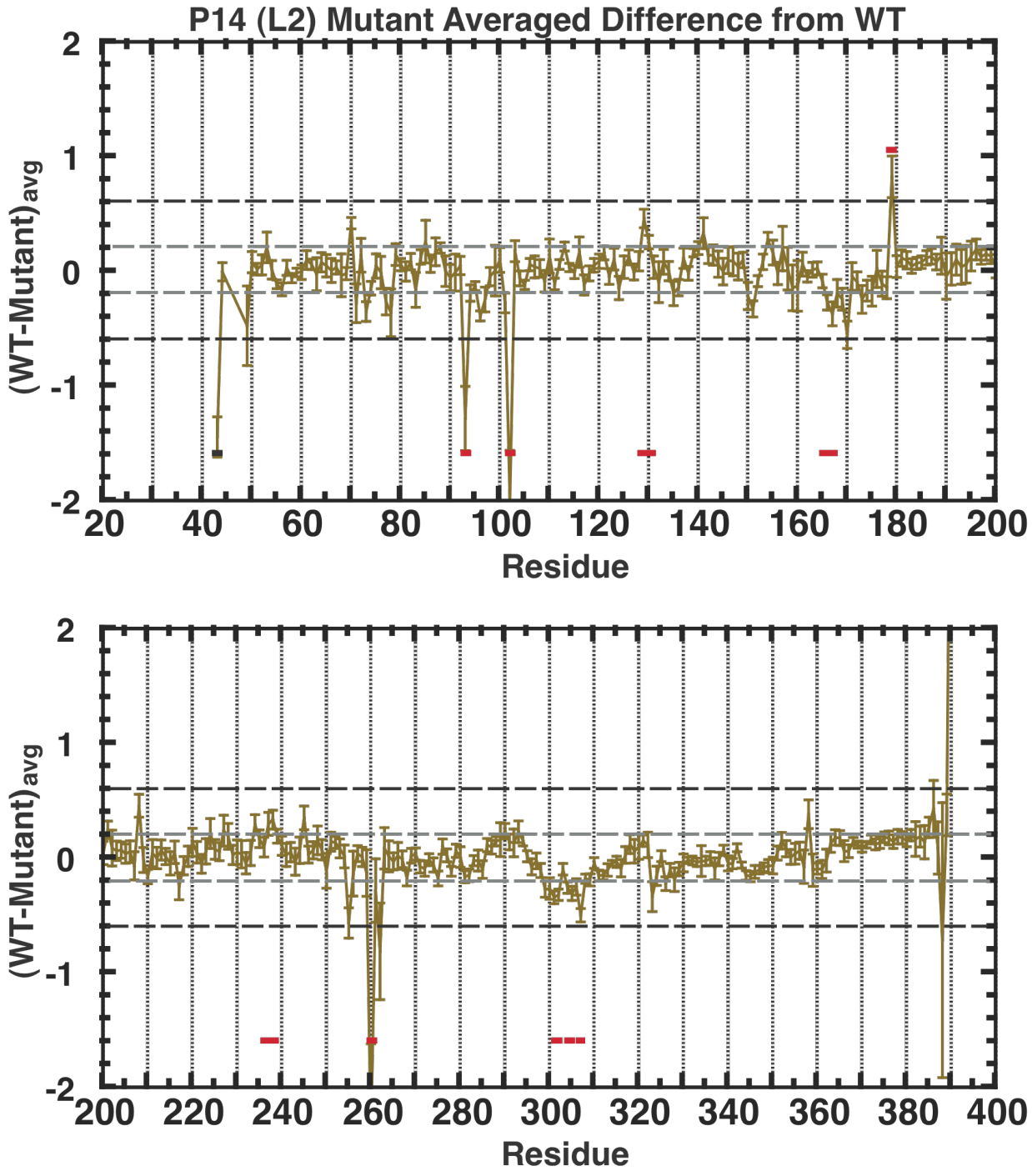
P14 (L2) Mutant Averaged Difference from WT
(WT-Mutant)avg
Residue
2
1
0
-1
-2
20
40
60
80
100
120
140
160
180
200
220
240
260
280
300
320
340
360
380
400

Figure S15

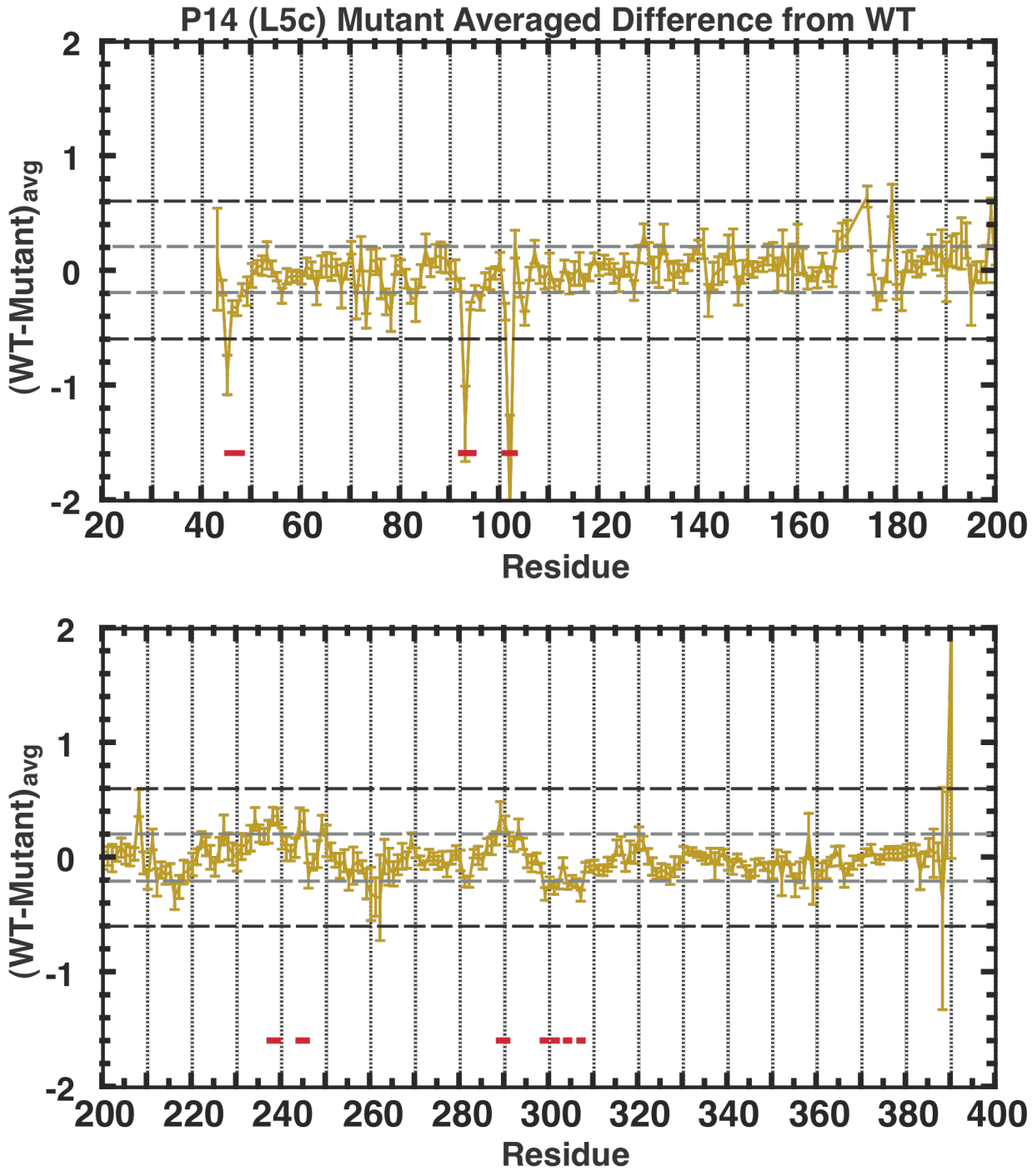
P14 (L5c) Mutant Averaged Difference from WT
(WT-Mutant)avg
Residue
2
1
0
-1
-2
20
40
60
80
100
120
140
160
180
200
220
240
260
280
300
320
340
360
380
400

Figure S16

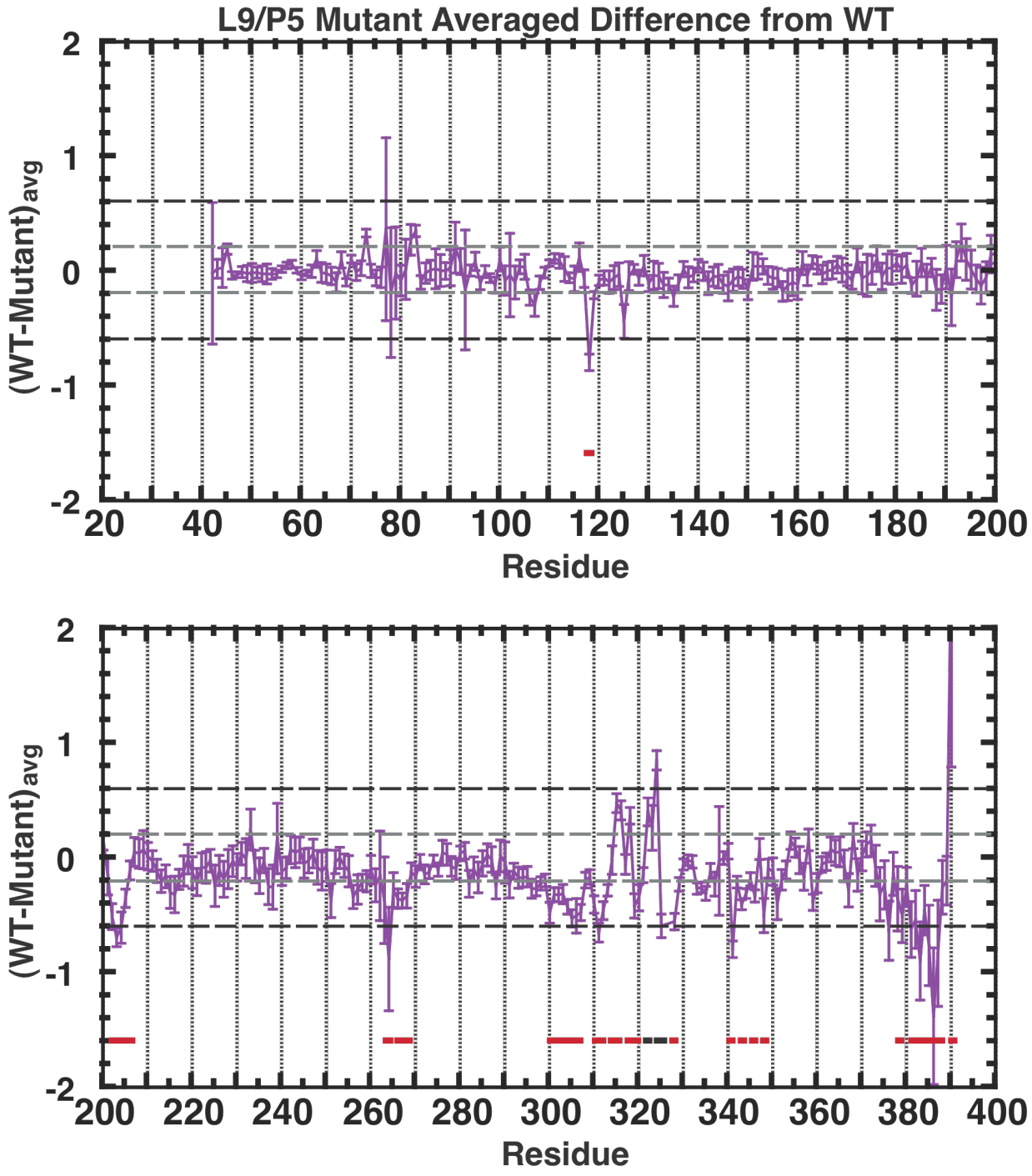
L9/P5 Mutant Averaged Difference from WT
(WT-Mutant)avg
Residue
2
1
0
-1
-2
20
40
60
80
100
120
140
160
180
200
220
240
260
280
300
320
340
360
380
400

Figure S17

REFERENCES

1. Uchida, T., Takamoto, K., He, Q., Chance, M. R., and Brenowitz, M. (2003) Multiple monovalent ion-dependent pathways for the folding of the L-21 Tetrahymena thermophila ribozyme, *J Mol Biol 328*, 463-478.
2. Das, R., Laederach, A., Pearlman, S. M., Herschlag, D., and Altman, R. B. (2005) SAFA: semi-automated footprinting analysis software for high-throughput quantification of nucleic acid footprinting experiments, *RNA 11*, 344-354.
3. Tijerina, P., Mohr, S., and Russell, R. (2007) DMS footprinting of structured RNAs and RNA-protein complexes, *Nat Protoc 2*, 2608-2623.
4. Shcherbakova, I., Mitra, S., Beer, R. H., and Brenowitz, M. (2008) Following molecular transitions with single residue spatial and millisecond time resolution, *Methods Cell Biol 84*, 589-615.